

# Mechanically-controlled multifaceted dynamic transformations in twisted organic crystal waveguides

Mehdi Rohullah,<sup>†</sup> Vuppu Vinay Pradeep,<sup>†</sup> Shruti Singh, and Rajadurai Chandrasekar\*

M. Rohullah, V. V. Pradeep, S. Singh and Prof. R. Chandrasekar

Advanced Photonic Materials and Technology Laboratory, School of Chemistry and Centre for Nanotechnology

University of Hyderabad, Prof. C. R. Rao Road, Gachibowli, Hyderabad 500 046, Telangana, India

E-mail: r.chandrasekar@uohyd.ac.in

<sup>#</sup> Equal contribution of authors

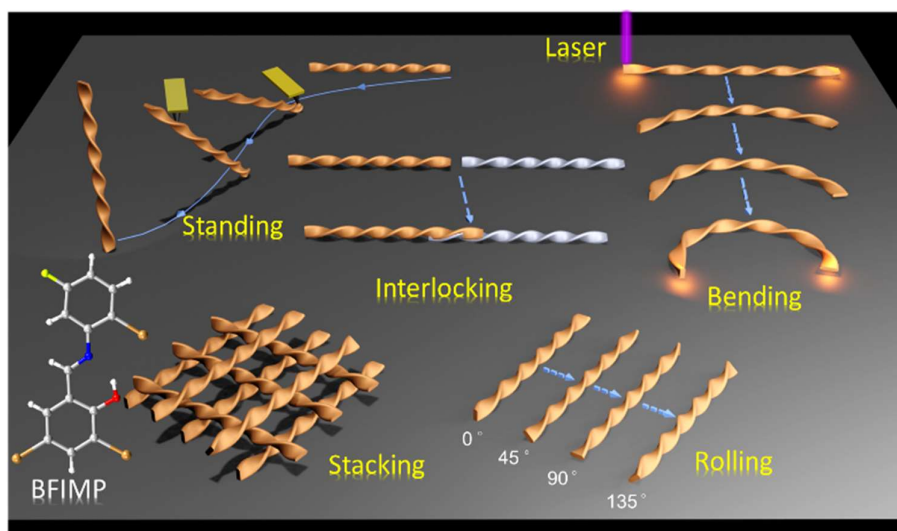
Supporting information for this article is given via a link at the end of the document.

**Abstract:** This study introduces mechanically induced novel phenomena such as standing, leaning, stacking, and interlocking behaviors in naturally twisted optical waveguiding microcrystals on a substrate. The twisted crystal self-assembled from 2,4-dibromo-6-(((2-bromo-5-fluorophenyl)imino)methyl)phenol is flexible and emits orange fluorescence. Crystal's mechanical flexibility in the perpendicular direction to (001) and (010) planes can be attributed to intermolecular interactions, including C-H $\cdots$ Br, N-H $\cdots$ O, C-H $\cdots$ O, and  $\pi\cdots\pi$  stacking interactions. Through a systematic process involving step-by-step bending and subsequent optical waveguiding experiments at each bent position, a linear relationship between optical loss and mechanical strain is established. Additionally, the vertical standing and leaning of these crystals at different angles on a flat surface and the vertical stacking of multiple crystals reveal the three-dimensional aspects of organic crystal waveguides, introducing light trajectories in a 3D space. Furthermore, the integration of two axially interlocked twisted crystals enables the coupling of polarization along their long axis. These novel crystal dynamics expand the horizons of crystal behavior and have the potential to revolutionize various applications, rendering these crystals invaluable in the realm of crystal-related science and technology.

## Introduction

Crystals exhibiting dynamic mechanical responses to external stimuli have attracted significant interest among researchers in fields such as sensor technology<sup>1-3</sup>, switchable materials<sup>4-6</sup>, actuator development<sup>7-11</sup>, artificial muscle design<sup>12,13</sup>, robotics<sup>14-16</sup>, and the fabrication of smart optical waveguides<sup>17-23</sup>. The dynamic macroscopic behaviors of organic crystals are often correlated with varying internal structural changes caused by trans-cis isomerization<sup>24-26</sup>, cycloadditions<sup>27</sup>, protonation/deprotonation<sup>28</sup>, electrocyclic reactions and phase transitions<sup>29-31</sup>. Within the realm of responsive materials, the mechanical activation of motions in molecular crystals includes, bending<sup>27, 32-37</sup>, twisting<sup>27,36-38</sup>, curling<sup>39</sup>, crawling<sup>40,41</sup>, jumping<sup>42,43</sup>, walking<sup>44</sup>, and rolling<sup>35,37,44</sup>. In the majority of reported cases, crystals tend to display only one or two of these dynamic motions, underscoring the limited versatility and diversity in their behaviors.

Further, researchers working in the domain of materials science, solid-state chemistry, and crystal engineering, are actively engaged in discovering novel mechanically triggered/controlled dynamic phenomena within soft crystals, distinct from those previously documented. The observation of novel crystal dynamics such as *standing*, *leaning*, *stacking*, and *interlocking* represents a significant advancement in our understanding of material behavior at the microscale. In our recent observations, we have noticed that microscale twisted crystals apart from *rolling* and *bending*, have a notable tendency to *stand* diagonally when downward mechanical force is applied to one of their crystal tips. Moreover, these crystals exhibit dynamic *leaning* behaviors and varying tilt angles in response to changes



**Scheme 1: Multifaceted dynamic transformations in twisted crystals.** Graphical illustration depicting standing, bending, rolling, stacking, and interlocking of twisted organic molecular single crystals of BFIMP.

in the magnitude of the applied mechanical force. Further, a twisted crystal can be intentionally bisected into two separate pieces and subsequently reconnected through a meticulous, screw-like mechanical *interlocking* mechanism, resulting in the seamless restoration of a single, continuous crystal structure. Moreover, an organized assembly of twisted crystals can be strategically stacked atop another assembly, with the inherent twists serving as delicate locking points between the lower and upper crystal arrays. This innovative approach, involving mechanical-force triggered, controlled, and multifaceted dynamic transformations such as *bending*, *rolling*, *standing*, *leaning*, *stacking*, and *interlocking*, reveals the inherent adaptive capabilities of twisted crystals. These findings hold the promise of unlocking new opportunities for the development of advanced microscale light guiding and sensing technologies.

In this report, we present a range of exceptional and unusual mechanically-triggered dynamic effects in all three dimensions (3D) viz. bending, rolling, standing, standing, stacking, and interlocking of a novel twisted crystal of 2,4-dibromo-6-(((2-bromo-5-fluorophenyl)imino)methyl)phenol (BFIMP). BFIMP exhibits orange fluorescence (FL). The unique twisted crystal exhibits high flexibility, primarily due to weak intermolecular interactions and  $\pi \cdots \pi$  interactions. The mechanically rollable crystal efficiently facilitates light propagation in both straight and highly curved geometries, exhibiting minimal optical loss. Remarkably, we demonstrate the mechanical repositioning of twisted crystals initially grown parallel to the substrate plane, enabling them to adopt both *vertical* and *slanted* orientations at diverse angles, facilitating controlled light guidance at desired angles. A 3D array of crystal waveguides can be systematically generated by mechanically *stacking* them in a square grid configuration. The screw-like mechanical *interlocking* of two twisted optical waveguides was achieved through precise axial entwinement of the microcrystals' tips, extending the crystal waveguide's length. The 3D dynamic modulation of optical signal propagation trajectories in these mechanically responsive crystal waveguides not only underscores their practical utility but also plays a pivotal role in the advancement of sophisticated devices for applications in soft robotics, smart sensors, flexible optoelectronics, and organic photonics.<sup>45-</sup>  
51

## Results and Discussion

The compound BFIMP was synthesized through a Schiff base reaction between 2-bromo-5-fluoroaniline and 3,5-dibromosalicylaldehyde in methanol under sonication, resulting in an 82% yield of

an orange solid (as shown in Figure 1a, Figure S1, and S2). Subsequently, the obtained compound was subjected to crystallization in methanol, resulting in the formation of millimeter-sized acicular crystals (Figure 1b). In its solid-state form, BFIMP crystals exhibited a unique absorption spectrum featuring a broad band with a  $\lambda_{\text{max}}$  of  $\approx 435$  nm. The fluorescence (FL) spectrum centered at around 620 nm, with a

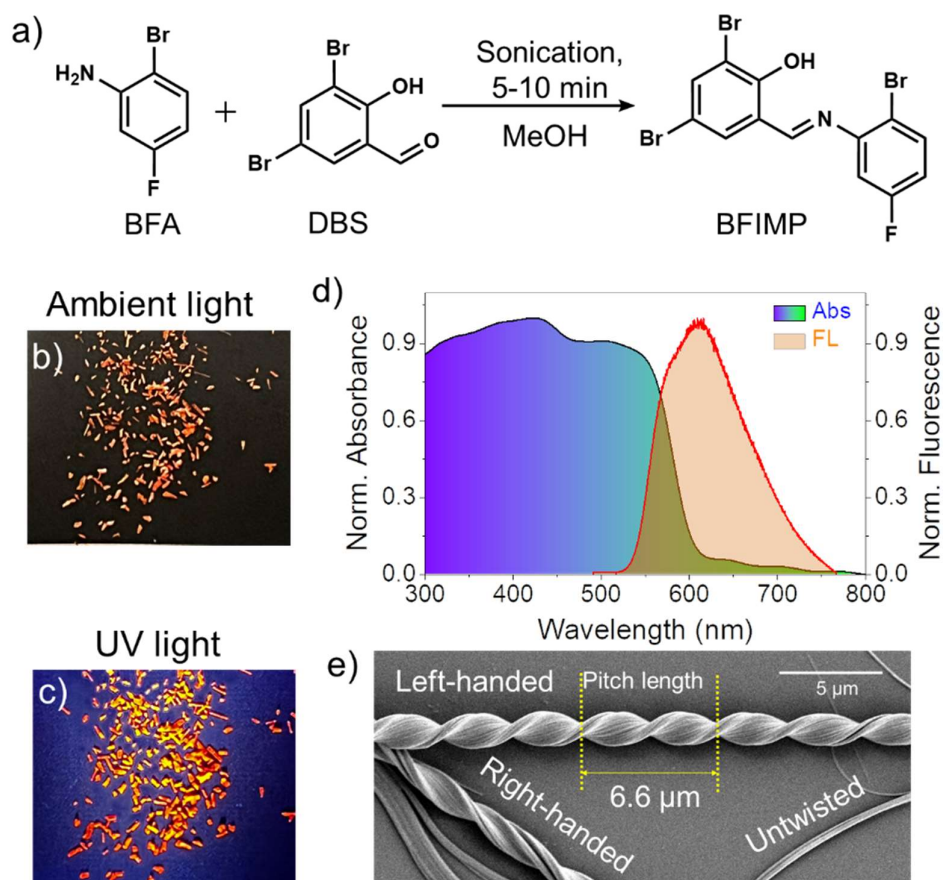


**Figure 1. Preparation, photophysical properties and microscopic data of the BFIMP.** a) Synthetic scheme of BFIMP. b,c) Photographs of macro crystals under ambient and UV light, respectively. d) Normalized absorption and emission spectra of BFIMP in solid-state. e) FESEM image displaying left, right-handed twisted, and untwisted morphology of BFIMP microcrystals.

bandwidth spanning from approximately 510 nm to 775 nm (Figure 1d). When exposed to UV light, the macrocrystals emitted a vibrant orange glow (Figure 1c).

The single X-ray crystal structure of as-grown millimeter-sized BFIMP crystals with a rectangular morphology showed the monoclinic space group,  $P2_1/n$  (CCDC number: 2300243; Table S1). In the crystal lattice, BFIMP molecules exhibited intramolecular O-H $\cdots$ N hydrogen bonding (1.863 Å, top view) and  $\pi\cdots\pi$  stacking interactions (3.683 Å, side view). As a result, the molecule demonstrated nearly planar geometry with minimal torsion angles between its benzene rings (0.64° and -2.15°, Figure 2a). Each molecule is surrounded by eight molecules with two types of Br $\cdots$ Br (3.589 Å, 3.690 Å), and F $\cdots$ Br (3.175 Å) intermolecular interactions and two molecules are in  $\pi\cdots\pi$  stacked manner (Figure 2b). The crystallographic analysis of BFIMP unveiled an antiparallel molecular orientation within the b and c planes (Figure 2c). When observed along the crystallographic c and b axes, the molecules adopted a slip-stacked arrangement involving  $\pi\cdots\pi$  interactions, as depicted in Figures 2d and 2e.

To facilitate a better understanding of the crystal's geometry, the primary facets of the mounted macrocrystal were determined to be (001), (010), and (100) through face indexing (Figure S3). The

correlation of identified facets with the crystal structure is given in Figure 2f. For the photonic and mechanical studies, the microcrystals were grown via a self-assembly approach from a 1 mg / 2 mL solution of BFIMP in ethyl acetate. The solution was drop casted onto a clean glass coverslip and covered with a Petri dish, thereby allowing the solution to evaporate slowly under ambient conditions. Interestingly, the resultant microcrystals were in twisted and as well as untwisted fashion with rectangular cross-sections when viewed under an optical microscope and field emission scanning electron microscope (FESEM) (Figure 1e and Figure S4). The EDAX analysis on twisted crystals further confirmed the presence of C, N, O, F and Br (Figure S5). The FL lifetime of the twisted microcrystals is about 0.51 ns (Figure S6).

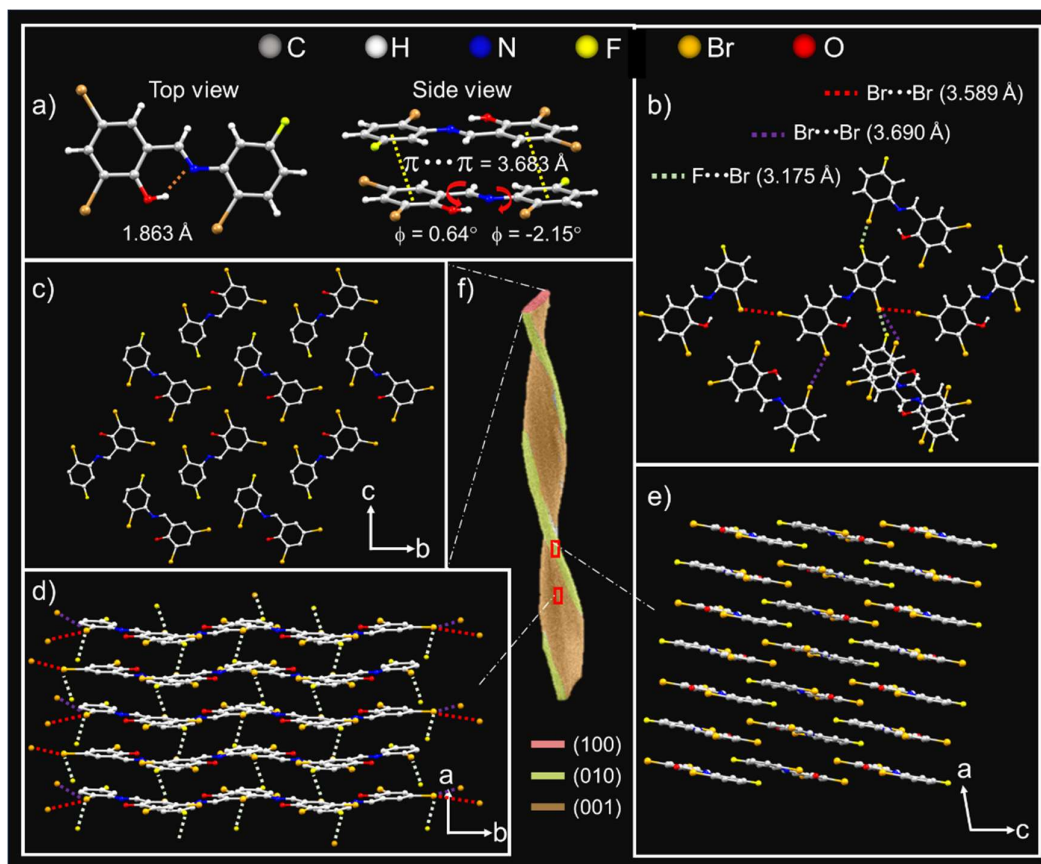


**Figure 2. Single-crystal X-ray diffraction analysis of BFIMP.** a) Top-view and side-view of BFIMP molecules. b) Each BFIMP molecule is surrounded by eight molecules via intermolecular interactions. The red and purple dotted line represents Br···Br interactions. The light green dotted lines represent F···Br interactions. c-e) The crystal packing of BFIMP along (100), (010), and (001) facets corresponds to the crystallographic a, b, and c axes, respectively. f) Color-coded FESEM image of a rectangular twisted BFIMP single crystal with three facets ((100), (010), and (001)) represented by three different colors.

Twisted crystals with varying rectangular cross-sections and twist periods (or) pitches ( $P$ ) were found (Figure S4). Twisting is characterized by a pitch,  $P = \pi / \theta$ , the length required to achieve a  $180^\circ$  rotation, where  $\theta$  is the twist per unit length. Both periodic and non-periodic pitch configurations were observed, indicating the coexistence of different twisting patterns (Figure 1e). Significantly, thicker crystals exhibited longer pitch lengths due to their increased rigidity, which acted to suppress the twisting

moment imposed by internal and external forces. Consequently, these crystals underwent untwisting and elongated their pitch lengths. Further, FESEM investigation unveiled the composite nature of these twisted and straight crystals, revealing their formation from an aggregation of numerous nanofibers. This crucial observation suggests that intergrowing nanocrystallites generate strain, contributing to the formation of twisted crystals. This finding aligns with our recent work on twisted crystals<sup>35</sup>, further confirming their intricate construction and reinforcing our understanding of their complex morphology. Both the right- and left-handed twisted crystals were found along with untwisted geometry (Figure 1e). A recent mechanistic study on twisted benzamide crystals provided insights into the growth mechanism, elucidating the role of orientationally mismatched nanofibers<sup>52</sup>. It was determined that cooperative interactions among these fibers, along with resulting interfacial strain, serve as the driving forces behind the spontaneous twists observed during crystal growth.

The BFIMP crystal demonstrates orange FL at its tips when exposed to UV light, confirming its optical waveguiding capabilities (Figure S7). To evaluate its mechanical flexibility and explore how bending affects its light-guiding properties, we excited a 195  $\mu\text{m}$  long straight twisted crystal at various positions and recorded the FL spectra at a fixed terminal (Figures 3a and 3b). The obvious gradual increase in FL intensity while decreasing the optical path length of the propagating light allowed us to investigate its optical loss in its straight and curved geometry. The overlap between absorption and emission spectra facilitated self-absorption of FL, leading to a gradual cutoff in the 510-540 nm region

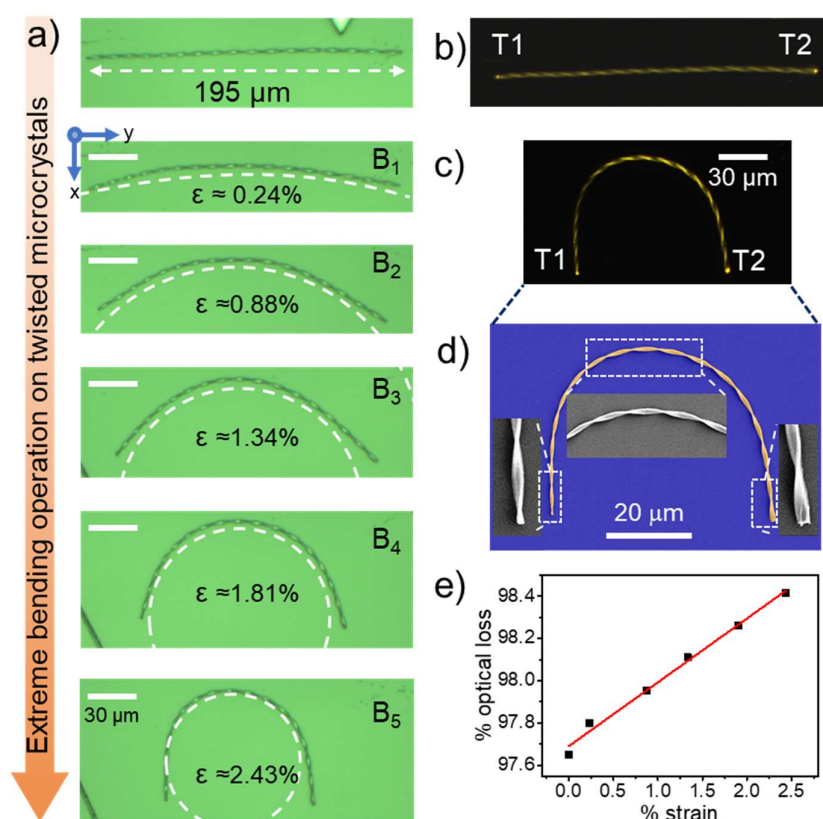


**Figure 3. Autonomous micromechanical bending of twisted crystal.** a) Optical images of a straight twisted microcrystal of length  $\approx 195 \mu\text{m}$  with its subsequent bent geometries (B1-B5) and respective mechanical strain ( $\epsilon$ ). b) The FL image of microcrystal in straight geometry. c,d) The FL and FESEM image of the corresponding crystal in B5 curved geometry. The inset shows the zoomed-in view of the outlined portions. e) The plot of the % optical loss versus the % strain caused due to bending of the crystal.

depending on the optical path length of the waveguide. The optical loss of the waveguide was estimated from the plot against  $I_{\text{tip}}/I_{\text{body}}$  and the propagation length  $D$  using the equation,  $I_{\text{tip}}/I_{\text{body}} = e^{-\alpha'D}$ , where  $\alpha'$  is the optical loss coefficient (Figure S7). The optical loss coefficient  $\alpha'$  was estimated to be  $0.11553 \text{ dB } \mu\text{m}^{-1}$  for straight twisted microcrystal.

Unlike untwisted crystals, the twisted geometry requires the bending of (010) and (001) facets. Initially, a mechanical force was applied along the x-direction to both termini using an AFM cantilever tip, resulting in the formation of a curved geometry (Supporting Video S1). The retention of this curved configuration upon the removal of mechanical force revealed the pseudoplastic properties of these microcrystals (Figure 3a). The mechanical strain ( $\epsilon$ ) acquired after the first bending (b1) was estimated to be 0.24%. Later, the curved crystal was excited at the left terminal (T1) and the FL spectra were recorded at both terminals T1 and T2, respectively. The percentage of optical loss was calculated using the equation  $\% \text{optical loss} = \frac{s_1 - s_2}{s_1} \times 100$ , where  $s_1$  and  $s_2$  represent the areas under the FL spectra collected at terminals T1 and T2, respectively. To examine the influence of the radius of curvature of the twisted crystal on the optical loss, stepwise bending, followed by mechanical and photonic studies was performed (Figure 3a,b). After each bend (B<sub>1</sub> to B<sub>5</sub>) the strain was calculated using the equation  $\epsilon = \left( \frac{\text{thickness}}{\text{diameter}} \right) \times 100$  and simultaneously, FL spectra were collected at terminal T2 by exciting at terminal T1. The FL image and the color-coded FESEM image of extremely bent geometry B<sub>5</sub> of the crystal are depicted in Figure 3c,d. Plotting mechanical strain against the percentage of optical loss revealed a linear correlation between these parameters (Figure 3e).

The twisted geometry of the microcrystals enables positioning them standing vertically on the substrate, exploiting the differences in height profile and surface attachment (Figure 4a). Specifically, the (010) and (001) facets of the linear twisted crystal align parallel to the substrate, while the (100) facet with a rectangular cross-section is oriented perpendicular to the substrate plane. To perform the controlled experiment, the twisted crystal of length  $\approx 92 \mu\text{m}$  was selected and its waveguiding ability was studied by exciting the crystal at the right terminal and recording the FL spectra at the left terminal (Figure 4b). The aim was to control the slanting angle of the crystal and investigate its photonic attributes. For this, the AFM tip was placed on the right terminal and gently pressed down (-z direction). As a result, the left end of the crystal lifted in the +z direction at an angle of  $10^\circ$ . The crystal's leaning angle was controlled by placing the AFM cantilever tip below the microcrystal and slowly moving in the +z direction. The microcrystal with different leaning angles of  $\approx 10^\circ$ ,  $\approx 17^\circ$ ,  $\approx 44^\circ$ ,  $\approx 58^\circ$ ,  $\approx 82^\circ$  was subjected to laser light (405 nm) by exciting the crystal at the bottom terminal. As the tilt angle increases, the recorded FL intensity at the top terminal increases (Figure 4a, inset). The corresponding FL images of the crystal clearly show the defocused top terminal of the leaning crystal with different tilt angles (Figure 4b). These innovative mechanical micromanipulation steps allowed the focusing of guided microlight at various angles in 3D space.

Further, a long-twisted microcrystal was chosen and was cut into different-sized smaller twisted crystals (s1 to s8; here 's' refers to standing). Later, the microcrystals were sequentially, vertically placed at different angles following the aforementioned mechanical operations (Figure 4c; Supporting Video S2). The FL image upon exposure to UV light depicts bright illumination of standing crystals with different heights (Figure 4e). The corresponding FESEM image ( $40^\circ$  tilt-view) clearly shows the vertically positioned twisted microcrystals on the substrate (Figure 4d). Interestingly, these standing twisted crystals orientation was

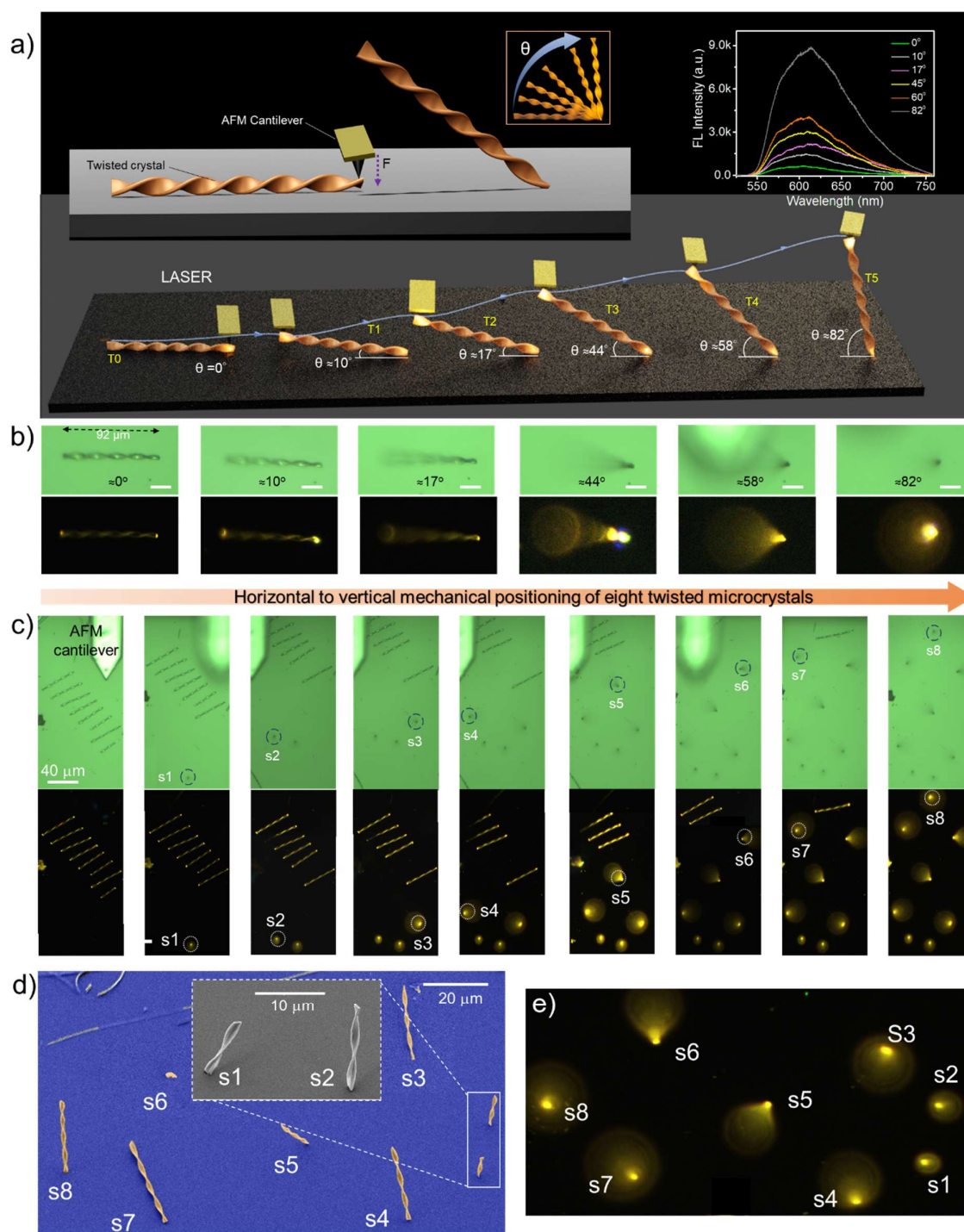


**Figure 4. Autonomous micromechanical standing/ slanting of twisted microcrystals.** a) Graphical representation depicting the mechanism of standing of microcrystal using the AFM cantilever tip. The images below show the microcrystals with various tilt angles (T0 to T7; T stands for tilt). b) The sequential confocal and FL images showing the slanted twisted microcrystal at various angles. The FL spectra are shown in the right-side inset of (a). c) The sequential confocal images of twisted microcrystals showing the vertical standing of 8 different-sized twisted microcrystals (s1-s8; s refers to standing) on a glass substrate and the corresponding FL images. d) Color-coded FESEM images reveal the standing of 8 twisted crystals with various tilt angles. The inset shows the zoomed-in image of standing crystals s1 and s2. e) The corresponding FL image under confocal setup.

firm even in high vacuum conditions like an SEM chamber. The crystals are resolutely standing even after 2 months. The close-up FESEM image of the crystals s1 and s2 displays the contact of the rectangular cross-section (facet 100) of the crystal bottom terminal with the substrate which explains the reason behind the leaning of the crystal on the substrate (inset, Figure 4d).

To assess the influence of the substrate on these unusually standing crystals, experiments were conducted by transferring twisted microcrystals (assisted by an AFM tip) from the original borosilicate glass substrate onto different substrates. These substrates included indium tin oxide-coated polyethylene terephthalate (ITO-PET), silicon, gold-coated glass, and aluminum foil. Subsequently, employing the aforementioned mechanical manipulation procedures, the microcrystals were vertically positioned on these various substrates, thereby confirming the versatility of this distinctive crystal behavior (Figure S9).

The 3D stacking of BFIMP crystals demands precise handling of microcrystals to prevent damage during the lifting, dropping, and integration stages. The layer-by-layer stacking process involves incorporating BFIMP crystals with different aspect ratios onto a borosilicate glass substrate. For the first layer, three crystals (C1, C2, and C3) with approximate lengths of 94  $\mu\text{m}$ , 89  $\mu\text{m}$ , and 106  $\mu\text{m}$  were selected (Supporting Video S3). These crystals were carefully aligned parallel to each other in the y-direction using an AFM cantilever tip (Figure 5a). As we progressed to subsequent layers, the placement of microcrystals on top of the existing layer required meticulous mechanical control. With an increasing number of layers, the complexity of aligning the crystals at specific angles significantly intensified, posing a substantial challenge in the stacking process. For the second layer, two twisted microcrystals, C4 and C5, each with

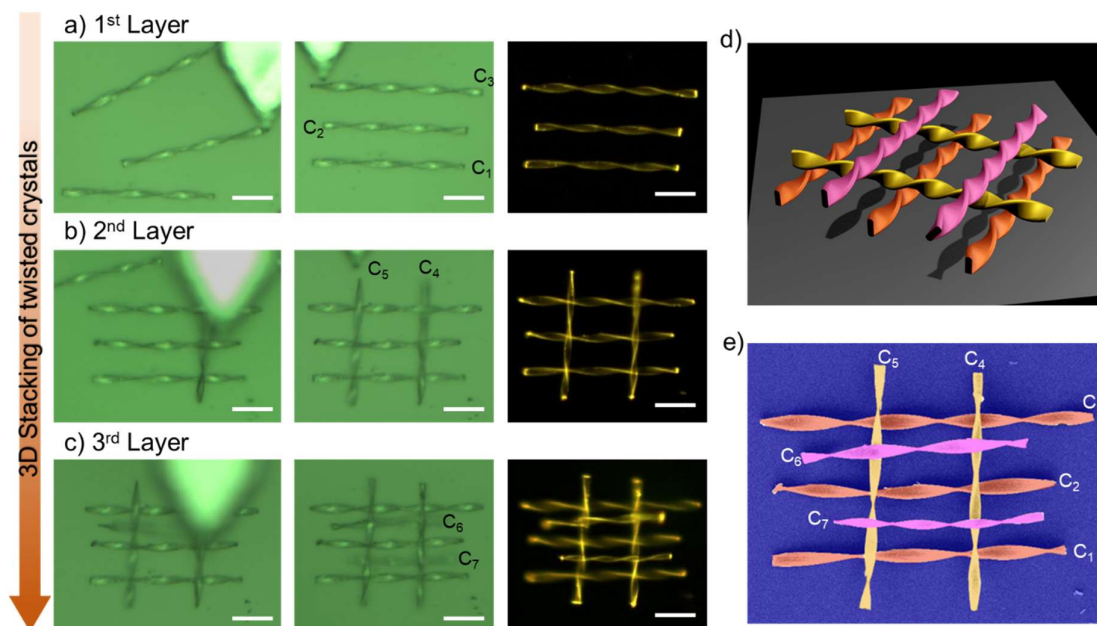


**Figure 5. Demonstration of 3D stacking of twisted microcrystals.** a-c) The sequential confocal images of twisted microcrystals showing the stacking (crystals C1 to C7) operations on a glass substrate. The corresponding FL images after each layer addition. d) Graphic and e) color-coded FESEM image of 3-layered stacked microcrystals.

lengths of approximately 77  $\mu\text{m}$  and 75  $\mu\text{m}$ , were successfully stacked vertically along the x-direction on the first layer, as shown in Figure 5b. Finally, another pair of crystals, C6 and C7, with lengths of about 72  $\mu\text{m}$  and 67  $\mu\text{m}$ , were precisely positioned perpendicular to the second layer while remaining parallel to the first layer in the horizontal (y-direction). It's noteworthy that the stacked crystals remained intact and stable even after undergoing a gold coating process and were observed under SEM conditions.

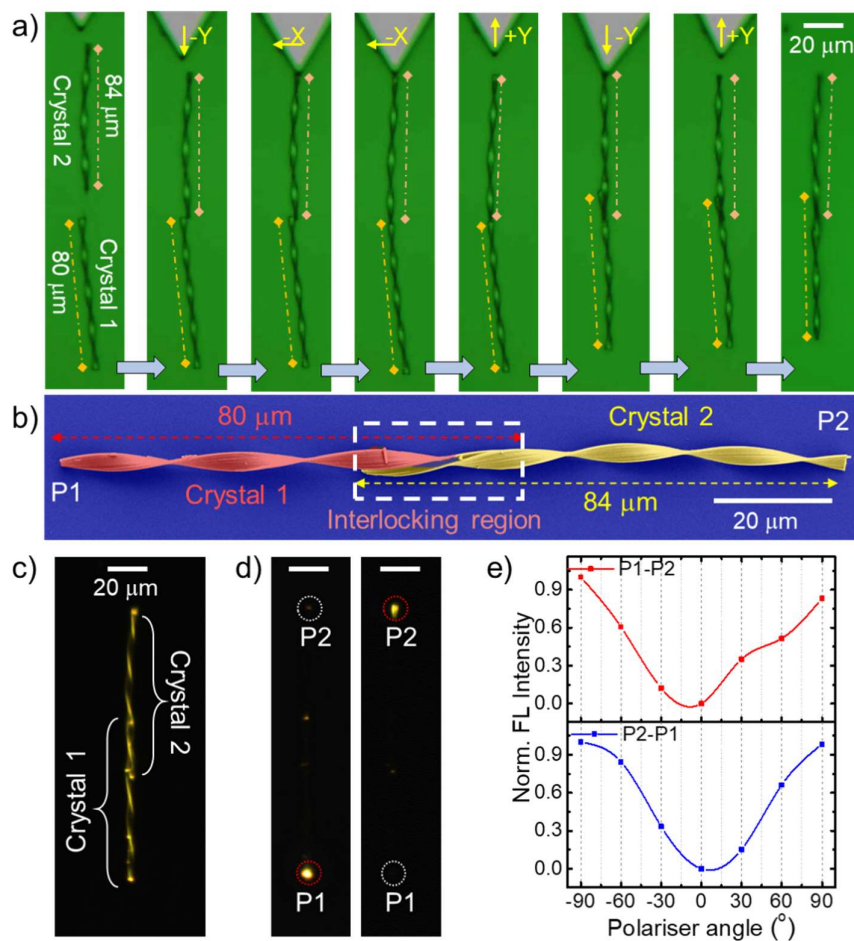


**Figure 6. Construction of interlocked microcrystals and their optical performance.** a) Confocal optical image displaying micromanipulation of two twisted microcrystals (crystals 1 and 2) to create an axially interlocked crystal. b) False color-coded FESEM image of axially connected twisted microcrystal. The white dashed box shows the interlocking region. c) FL image of interlocked crystal on exposure to UV light. d) FL image of interlocked microcrystals excited at terminal P1 and P2 and recorded the FL spectra at another end (red dotted circle). e) FL intensity recorded at terminal P2 for the input given at terminal P1 by changing polarizer angle ( $-90^\circ$  to  $+90^\circ$ ) for the interlocked crystal and vice versa.

The interlocking of two twisted crystal termini at the microscale demands precise handling and the careful selection of appropriate crystals. In this experiment (Supporting Video S4-S6), we selected two crystals, referred to as crystal 1 and crystal 2, each with approximate lengths of 80  $\mu\text{m}$  and 84  $\mu\text{m}$ . These crystals were positioned head-to-head in an axial manner. Their

orientation was adjusted to bring the dark contrast region of crystal 2 near the bright contrast region of crystal 1 (as depicted in Figure 6a). Subsequently, the crystals were gently manipulated first in the -y direction and then in the -x direction using an AFM cantilever tip to entwine the two crystals into a single unit. A close examination of the crystal under FESEM imaging clearly shows the axial connection (interlock) of the tips of crystals 1 and 2, as seen in Figure 6b. Furthermore, upon exposure to UV light, the crystal exhibits a bright yellow FL at its terminals, confirming its capability to function as a waveguide under interlocked conditions (Figure 6c and 6d).

To determine the polarization direction of the guided output light through the interlocked crystal waveguides, we excited crystal 1's P1 terminal using a 405 nm laser. This generated FL that transduced through the interlocked crystal, reaching crystal 2's P2 terminal, as depicted in Figure 6d (left). The intensity of the output light at crystal 2's P2 terminal exhibited a smooth variation as the polarizer angle was adjusted from  $-90^\circ$  to  $+90^\circ$ . The presence of maxima and minima in the spectral intensity, perpendicular to each other, confirms that the detected light is polarized, as shown in Figure 6e. The experiment was performed by exciting crystal 2's P2 terminal and collecting the output at crystal 1's P1 end also showed similar results. Moreover, the mirror-like, light-reflecting facets of the crystal substrate contributed to the appearance of optical modes in the FL spectrum of the output light (Figure S10). To assess the reproducibility of the interlocking process, we repeated the experiment with two additional twisted crystals of different lengths, measuring approximately  $50\ \mu\text{m}$  and  $83\ \mu\text{m}$ . Following the required micromechanical operations, these crystals successfully formed interlocked structures, as depicted in Figure S11.

## Conclusion

This study unveiled the novel mechanically-driven dynamics of organic twisted crystals, highlighting their remarkable abilities to stand vertically, lean, stack, and interlock, in conjunction with their known bending and rolling behaviors. Importantly, these crystals efficiently guide light along dynamic trajectories, greatly enhancing their versatility for various applications in the realm of nanophotonics, optoelectronics and nanorobotics. Our unique experiment established a linear correlation between mechanical strain and the waveguide's optical loss, revealing the vital connection between these parameters. The meticulous 3D stacking of crystals in three vertical layers demonstrated the remarkable capabilities of AFM-assisted mechanical micromanipulation, while our ability to position the crystals vertically at various angles on several substrates showcased their versatility and exceptional crystal dynamics.

Furthermore, our achievement of axially integrating two twisted crystals by precisely positioning them head-to-head, leveraging their similar cross sections, represents an innovative approach to extending the length of these crystals in one dimension. Axially interlocked crystal waveguides have exhibited a remarkable capacity to dynamically modulate the polarization state of the transmitted light, rendering these crystals a highly promising candidate for optical applications where precise polarization control is of paramount importance.

The remarkable three-dimensional control of crystal orientation not only expands the capabilities of these dynamic crystals but also holds immense potential for enhancing optical technologies, making them highly adaptable in various cutting-edge applications.

### Acknowledgments

RC thanks SERB-New Delhi (SERB-STR/2022/00011) and the University of Hyderabad-Institution of Eminence Scheme (UoH-IoE) [MHRD (F11/9/2019-U3(A))] for research funding MR and VVP thank CSIR for the fellowship.

### Author contributions

VVP and SS synthesized and characterized the molecule, and performed the optical waveguiding experiments, micromechanical bending and rolling of twisted microcrystals under the supervision of RC. VVP and MR carried out the mechanical micromanipulation and photonic studies of standing, 3D stacking and interlocked twisted microcrystals under the supervision of RC. All authors discussed the results and wrote the paper. The authors declare no conflict of interest.

**Keywords:** 3D stacked crystals • interlocked crystals • crystal dynamics • dynamic optical waveguides • standing/leaning crystal • twisted crystal

### References

- [1] H. Koshima, *Mechanically Responsive Materials for Soft Robotics*, Wiley-VCH Verlag, Weinheim, Germany (2020).
- [2] Spagnolo, G. S., Cozzella, L. & Leccese, F. Underwater Optical Wireless Communications: Overview. *Sensors* **20**, 2261 (2020).
- [3] Kumar, A. V. et al. Amphibian-like Flexible Organic Crystal Optical Fibers for Underwater/Air Micro-Precision Lighting and Sensing. *Angew. Chem. Int. Ed.* **62**, e202300046 (2023).
- [4] Kitagawa D. & Kobatake, S. Photoreversible current ON/OFF switching by the photoinduced bending of gold-coated diarylethene crystals. *Chem. Commun.* **51**, 4421 (2015).
- [5] Sato, O. Dynamic molecular crystals with switchable physical properties. *Nat. Chem.* **8**, 644 (2016).
- [6] Dharmarwardana, M. et al. Rapidly Reversible Organic Crystalline Switch for Conversion of Heat into Mechanical Energy. *J. Am. Chem. Soc.* **143**, 5951 (2021).
- [7] Kobatake, S., Takami, S., Muto, H., Ishikawa, T. & Irie, M. Rapid and reversible shape changes of molecular crystals on photoirradiation. *Nature* **446**, 778 (2007).
- [8] Zhu, L., Al-Kaysi, R. O., Dillon, R. J., Tham, F. S. & Bardeen, C. J. Crystal Structures and Photophysical Properties of 9-Anthracene Carboxylic Acid Derivatives for Photomechanical Applications. *Cryst. Growth Des.* **11**, 4975 (2011).
- [9] Zhu, L. et al. Improved Solid-State Photomechanical Materials by Fluorine Substitution of 9-Anthracene Carboxylic Acid. *Chem. Mater.* **26**, 6007 (2014).
- [10] Wani, O. M., Zeng, H. & Priimagi, A. A light-driven artificial flytrap. *Nat. Commun.* **8**, 15546 (2017).
- [11] Wang, H. et al. Positive/Negative Phototropism: Controllable Molecular Actuators with Different Bending Behavior. *CCS Chem.* **3**, 1491 (2021).

- [12] Takashima, Y. et al. Expansion–contraction of photoresponsive artificial muscle regulated by host–guest interactions. *Nat. Commun.* **3**, 1270 (2012).
- [13] Iwaso, K., Takashima, Y. & A. Harada. Fast response dry-type artificial molecular muscles with [c2] daisy chains. *Nat. Chem.* **8**, 625 (2016).
- [14] Ilievski, F., Mazzeo, A. D., Shepherd, R. F., Chen, X. & Whitesides, G. M. Soft Robotics for Chemists. *Angew. Chem. Int. Ed.* **50**, 1890 (2011).
- [15] Rus, D. & Tolley, M. T. Design, fabrication and control of soft robots. *Nature* **521**, 467 (2015).
- [16] Ahmed, E., Karothu, D. P., Warren, M. & Naumov, P. Shape-memory effects in molecular crystals. *Nat. Commun.* **10**, 3723 (2019).
- [17] Takazawa, K., Kitahama, Y., Kimura, Y. & Kido, G. Optical waveguide self-assembled from organic dye molecules in solution. *Nano Lett.* **5**, 1293 (2005).
- [18] Chandrasekar, N., Mohiddon, Md. A. & Chandrasekar, R. Organic Submicro Tubular Optical Waveguides: Self-Assembly, Diverse Geometries, Efficiency, and Remote Sensing Properties. *Adv. Opt. Mater.* **1**, 305 (2013).
- [19] Liu, H., Lu, Z., Zhang, Z., Wang, Y. & Zhang, H. Highly Elastic Organic Crystals for Flexible Optical Waveguides. *Angew. Chem. Int. Ed.* **57**, 8448 (2018).
- [20] Annadhasan, M. et al. Micromanipulation of Mechanically Compliant Organic Single-Crystal Optical Microwaveguides. *Angew. Chem. Int. Ed.* **59**, 13821(2020).
- [21] Annadhasan, M. et al. Mechanophotonics: Flexible Single-Crystal Organic Waveguides and Circuits. *Angew. Chem. Int. Ed.* **59**, 13852 (2020).
- [22] Lu, Z. et al. Optical Waveguiding Organic Single Crystals Exhibiting Physical and Chemical Bending Features. *Angew. Chem. Int. Ed.* **59**, 4299 (2020).
- [23] Annadhasan, M., Pradeep, V. V., Kumar, A. V., Ravi, J. & Chandrasekar, R. Integrating Triply- and Singly-Bent Highly Flexible Crystal Optical Waveguides for Organic Photonic Circuit with a Long-Pass-Filter Effect. *Small Struct.* **3**, 2100163 (2022).
- [24] Peng, J. et al. Light-Induced Bending of Needle-Like Crystals of Naphthylvinylbenzoxazole Triggered by *trans–cis* Isomerization. *Chem. Asian. J.* **13**, 1719 (2018).
- [25] Al-Kaysi, R. O. et al. Chemical reaction method for growing photomechanical organic microcrystals. *Cryst. Eng. Comm.* **17**, 8835 (2015).
- [26] Halabi, J. M. et al. Spatial Photocontrol of the Optical Output from an Organic Crystal Waveguide. *J. Am. Chem. Soc.* **141**, 14966 (2019).
- [27] Gupta, P., Karothu, D. P., Ahmad, E., Naumov, P. & Nath, N. K. Thermally Twistable, Photobendable, Elastically Deformable, and Self-Healable Soft Crystals. *Angew. Chem. Int. Ed.* **57**, 8498 (2018).
- [28] Takanabe, A. et al. Optical Activity and Optical Anisotropy in Photomechanical Crystals of Chiral Salicylidenephenylethylamines. *J. Am. Chem. Soc.* **138**, 15066 (2016).
- [29] Zheng, Y., Jia, X., Li, K., Xu, J. & Bu, X.-H. Energy Conversion in Single-Crystal-to-Single-Crystal Phase Transition Materials *Adv. Energy Mater.* **12**, 2100324 (2022).
- [30] Sakai, T., Kurakazu, M., Akagi, Y., Shibayama, M. & Chang, U. Effect of swelling and deswelling on the elasticity of polymer networks in the dilute to semi-dilute region. *Soft Matter* **8**, 2730 (2012).
- [31] Taniguchi, T., Sato, H., Hagiwara, Y., Asahi, T. & Koshima, H. Photo-triggered phase transition of a crystal. *Commun. Chem.* **2**, 19 (2019).
- [32] Yu, Y., Nakano, M. & T. Ikeda. Directed bending of a polymer film by light. *Nature* **425**, 145 (2003).
- [33] Ikeda, T., Mamiya, J. & Yu, Y. Photomechanics of Liquid-Crystalline Elastomers and Other Polymers. *Angew. Chem. Int. Ed.* **46**, 506 (2007).
- [34] Good, J. T., Burdett, J. J. & Bardeen, C. J. Photomechanical control. *Small* **5**, 2902 (2009).

- [35] Rohullah, M., Pradeep, V. V., Ravi, J., Kumar, A. V. & Chandrasekar, R. Micromechanically-Powered Rolling Locomotion of a Twisted-Crystal Optical-Waveguide Cavity as a Mobile Light Polarization Rotor. *Angew. Chem. Int. Ed.* **02**, 114 (2022).
- [36] Tang, S., Ye, K. & Zhang, H. Integrating Low-Temperature-Resistant Two-Dimensional Elastic-Bending and Reconfigurable Plastic-Twisting Deformations into an Organic Crystal. *Angew. Chem. Int. Ed.* **61**, e202210128 (2022).
- [37] Liu, H. et al. A Flexible Organic Single Crystal with Plastic-Twisting and Elastic-Bending Capabilities and Polarization-Rotation Function. *Angew. Chem. Int. Ed.* **59**, 12944 (2020).
- [38] Tang, B., Yu, X., Ye, K. & Zhang, H. Manifold Mechanical Deformations of Organic Crystals with Optical Waveguiding and Polarization Rotation Functions. *Adv. Opt. Mater.* **10**, 2101335 (2022).
- [39] Kim, T., Al-Muhanna, M. K., Al-Suwaidan, S. D., Al-Kaysi, R. O. & Bardeen, C. J. Photoinduced Curling of Organic Molecular Crystal Nanowires. *Angew. Chem. Int. Ed.* **52**, 6889 (2013).
- [40] Uchida, E., Azumi, R. & Norikane, Y. Light-induced crawling of crystals on a glass surface. *Nat. Commun.* **6**, 7310 (2015).
- [41] Norikane, Y. et al. Photo-Induced Crawling Motion of Azobenzene Crystals on Modified Gold Surfaces. *Langmuir* **37**, 14177 (2021).
- [42] Skoko, Z., Zamir, S., Naumov, P. & Bernstein, J. The Thermosalient Phenomenon. “Jumping Crystals” and Crystal Chemistry of the Anticholinergic Agent Oxitropium Bromide. *J. Am. Chem. Soc.* **132**, 14191 (2010).
- [43] Lusi, M. & Bernstein, J. On the propulsion mechanism of “jumping” crystals. *Chem. Commun.* **49**, 9293 (2013).
- [44] Taniguchi, T. et al. Walking and rolling of crystals induced thermally by phase transition. *Nat. Commun.* **9**, 538 (2018).
- [45] Chandrasekar, R. Mechanophotonics—Mechanical Micromanipulation of Single-Crystals toward Organic Photonic Integrated Circuits. *Small* **17**, 2100277 (2021).
- [46] Chandrasekar, R. Mechanophotonics – a guide to integrating microcrystals toward monolithic and hybrid all-organic photonic circuits. *Chem. Commun.* **58**, 3415 (2022).
- [47] Chandrasekar, R. Advanced All-Organic Microphotonic Components and Integrated Circuits. *Adv. Opt. Mater.* **11**, 2301124 (2023).
- [48] Ravi, J. et al. Geometrically Reconfigurable, 2D, All-Organic Photonic Integrated Circuits Made from Two Mechanically and Optically Dissimilar Crystals. *Adv. Funct. Mater.* **31**, 2105415 (2021).
- [49] Ravi, J., Annadhasan, M., Kumar, A. V. & Chandrasekar, R. Mechanically Reconfigurable Organic Photonic Integrated Circuits Made from Two Electronically Different Flexible Microcrystals. *Adv. Funct. Mater.* **31**, 2100642 (2021).
- [50] Pradeep, V. V. et al. Mechanical Processing of Naturally Bent Organic Crystalline Microoptical Waveguides and Junctions. *Small* **17**, e2006795 (2021).
- [51] Pradeep, V. V., Kumar, A. V. & Chandrasekar, R. A Tandem Approach to Fabricate a Hybrid, Organic-Add-Drop Filter Using Single-Crystal Disk-Resonators and Pseudo-Plastic Crystal Waveguides. *Laser Photonics Rev.* DOI:10.1002/lpor.202300552 (2023).
- [52] Shtukenberg, A. G. et al. Crystals of Benzamide, the First Polymorphous Molecular Compound, Are Helicoidal. *Angew. Chem. Int. Ed.* **14**, 4577 (2020).